/

Metal Solution Precursors: Their Role During the Synthesis of MoVTeNb Mixed Oxide Catalysts

Jaime S. Valente,*[a] Etel Maya-Flores,[a] Héctor Armendáriz-Herrera,[a] Roberto Quintana-Solórzano [a] and José M. López Nieto [b]

Synthesized via the slurry method and activated at high temperature (873 K), MoVTeNb multimetallic mixed oxides are applied to catalyze the oxidative dehydrogenation of ethane to ethylene (ODHE). Mixed oxides typically contain M1 and M2 crystalline phases, the relative contribution of these phases and the respective catalytic behavior being notably influenced by the preparation conditions of the metallic aqueous solution precursor, given the complexity of the chemical interactions of metal species in solution. Thus, detailed in situ UV-Vis and Raman studies of the chemical species formed in solution during each step of the synthetic procedure are presented herein. The main role of vanadium is to form decavanadate ions, which interact with Mo species to generate an Anderson-type structure. When niobium oxalate solution is added into the MoVTe solution, a yellow-colored gel is immediately formed due to a common ion effect. When liquid and gel phases are separated, the M1 crystalline phase is produced solely from the gel phase. Attention is also devoted to the influence and role of each metal cation (Mo, V, Te and Nb) on the formation of the active M1 crystalline phase and the catalytic behavior in the ODHE. The catalyst constituted mostly of M1 crystalline phase is capable to convert 45 % of the fed ethane, with a selectivity to ethylene of around 90 %.

Introduction

In the mid-90s, Mitsubishi Chemical Co. presented two patents for producing acrylic acid and acrylonitrile from propane using Mo-V-Te-X based catalysts.[1,2] Since then, a large number of studies have been published regarding physicochemical and catalytic properties of these materials.[3-15] The discovery that propane can be transformed into acrylonitrile through a direct, multi-step transformation pathway at relatively low temperature, attracted a great deal of interest from academic and industrial communities as the activation of light hydrocarbons (i.e., C_1 to C_4) and their selective transformation into valuable products is still challenging.[16,25] Interestingly, despite the intrinsic chemical complexity of this multistep propane ammoxidation reaction, such multimetallic materials are basically constituted of two crystalline phases, to wit, orthorhombic and pseudo-hexagonal type structures, corresponding to the so-called M1 and M2 phases, respectively.[3,4] These phases, aside, can be produced by different methodologies after heat-treatment in inert atmosphere within the temperature range 823 - 923 K.

It has also been reported that ethylene can be selectively obtained out of the oxidative dehydrogenation of ethane (ODHE) applying Mo-V-Te-Nb mixed oxides catalysts.[15,26-35] In fact, MoVTeNbO mixed metal oxides have been claimed as the most effective catalysts for ethane ODH.[15,26-28] The best results achieved on these catalysts, *i.e.*, yield of *ca.* 75 %,[26,27] are actually higher than those reported previously over modified MoVNbO[36] mixed oxides or Mo_3VO_x catalysts.[37] They would correspond to similar catalytic systems in principle, nonetheless, important differences can be identified among them. In particular, the presence of the M1 crystalline phase has been identified as a key aspect in the high efficiency of MoVTeNbO catalysts.[27]

In the last two decades, Mo-V-Te-Nb multimetallic mixed oxide has been one of the most studied materials for usage in the partial oxidation of light hydrocarbons. Thus, one of the most important conclusions over the Mo-V-Te-Nb mixed oxide is the paramount role of Te-sites, since they favor not only the formation of M1 phase [27] but also the elimination of undesirable non-selective sites related to the formation of CO_x [28]. There are evidences that Te atoms provide structural stability to the solid because of their location into the hexagonal and heptagonal channels of the M1 structure. Elucidating the whole catalytic properties of such a multicomponent catalytic system is, however, fairly complex.

In the last years, many research efforts have been made to characterize physicochemical properties of the Mo-V-Te-Nb mixed metal oxide system to provide information to understand its outstanding high catalytic activity.[3-33] The nature of the active sites, which are responsible of the selective oxidation of low molecular weight hydrocarbons, has been widely investigated.[3,17,20,38-41] Diverse synthetic procedures to obtain this catalytic system[42-48] including hydrothermal synthesis, slurry method, solid state reaction[7] and physical vapor deposition,[46] among others.[42,45,47,48] Even though M1 and M2 crystalline phases are dominant, others might also appear, for instance, $(Mo_{0.93}V_{0.07})_5O_{14}$, MoO_3, $Mo_{0.91}Nb_{0.09}O_{2.8}$ and $TeMo_5O_{16}$.[49]

Synthesis parameters, particularly, temperature, time, concentration, gel composition and pH have a large influence on the resulting crystalline phase distribution and, hence, the catalytic activity.[43,49-51] Therefore, studying in detail the optimal synthesis parameters as well as the mechanism behind the formation of the active M1 phase is of a paramount importance. In the literature, few reports concerning the nature, response to synthesis conditions and chemical interactions of the metal aqueous species generated during synthesis can be found.[50,51] This work, therefore, aims to present a detailed study of the chemical species and their interaction in each step of the synthetic procedure. The slurry method was selected to synthesize the catalysts for simplicity reasons taking into consideration that it requires less time and lower temperatures than other methodologies. The prepared solutions at each step of synthetic procedure were subjected to analysis via spectroscopic UV-Vis and Raman analyses. In addition, the effect of the catalyst preparation conditions on the catalytic behaviour for the oxidative dehydrogenation of ethane (ODHE) was examined.

RESULTS AND DISCUSSION

UV-Vis and Raman spectroscopies of metals solutions

Figures 1 and 2 show the UV-Vis and Raman spectra, respectively, of metallic solutions at each preparation step (*vide* Section 2.1). The UV-Vis region scanned is associated with the electron transfer from oxygen *2p* orbitals to *3d* orbitals of transition metals in aqueous solution. The spectrum *a* in Figure 1, which corresponds to the colourless ammonium heptamolybdate (AHM) solution (0.046 $mmol_{AHM}/mL_{H2O}$, pH = 4.65), does not present absorption bands in the visible region. The spectrum, in fact, exhibits a single absorption band that extends from 285 to 350 nm (see inset). This band is attributed, according to the equilibrium species in aqueous solution at pH close to 4.98 and at room temperature,[52] to $[Mo_7O_{24}]^{6-}$ species, the Mo^{6+} ions being present in octahedral coordination. This broad band indicates a certain degree of polymerization or interconnectivity of $[Mo_7O_{24}]^{6-}$ species through Mo-O-Mo bonds. Thus, on the basis of the equilibrium diagram of HMA species in acidic medium,[52] several heptamolybdate species $[Mo_7O_{24}]^{6-} \leftrightarrow H[Mo_7O_{24}]^{5-} \leftrightarrow H_2[Mo_7O_{24}]^{4-} \leftrightarrow H_3[Mo_7O_{24}]^{3-}$ coexist at equilibrium, varying only in the hydration and protonation degree as a function of solution pH. In agreement with UV-Vis spectroscopy, the Raman spectrum of this solution (Figure 2, spectrum a) shows bands at 891 and 935 cm^{-1}, characteristic of the terminal Mo=O bending, antisymmetric Mo-O-Mo stretching, and symmetric and antisymmetric terminal stretching modes of $[Mo_7O_{24}]^{6-}$ species.[53] Trunschke *et al.*[50] have reported ammonium octamolybdate ions in a similar solution heated at 353 K. The partial transformation of ammonium heptamolybdate into ammonium octamolybdate was explained as a consequence of the decrease in pH (at 353 K), a transition that was not observed in the present study, however.

When adding ammonium metavanadate (AMV, 0.0787 $mmol_{AMV}/mL_{H2O}$) into the AHM solution, the pH slightly increased from 4.7 to 5.3. The UV–Vis spectrum of the resulting light yellow solution presented a broad band at about 450 nm (Figure 1, spectrum b), practically in between ultraviolet and

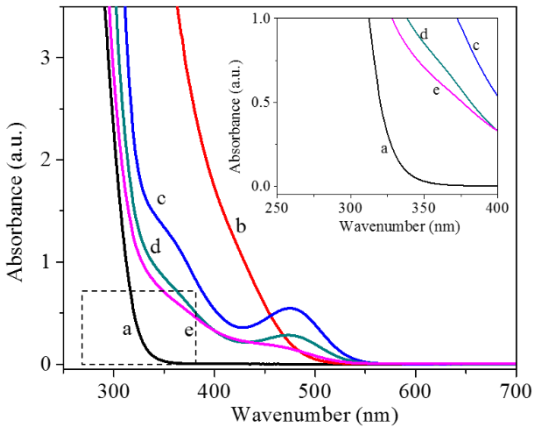

Figure 1. UV-Vis spectra of metals solution at different preparation steps: a) AHM; b) AMH-AMV; c) AHM-AMV-TA; d) AHM-AMV-TA-NbOx (pH=3.6); and e) AHM-AMV-TA-NbOx (pH=2.5).

visible regions. This broad band is assigned to the interaction between the *d* orbital of vanadium and the π system of the ligand[54] though it does not allow a clear identification of any Mo or V species. Furthermore, the absence of *d-d* transitions, in the 400-800 nm range, suggests a weak chemical interaction between Mo and V species, whilst reduced species of either Mo^{6+} or V^{5+} are not detected.[55] The yellow colour of the V^{5+} solution ($3d^0$) ions is due to electron transfers from the oxygen bonding orbitals to the vacant vanadium *d* orbitals. These charge transfer bands move towards the UV region when the crystal field splitting of *d* orbitals decreases.[56] Based on the

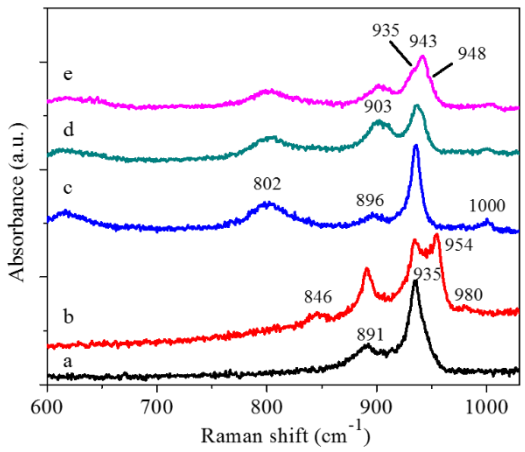

Figure 2. Raman spectra of metals solution at different preparation steps: a) AHM; b) AMH-AMV; c) AHM-AMV-TA; d) AHM-AMV-TA-NbO_x (pH=3.6); and e) AHM-AMV-TA-NbO_x (pH=2.5).

aqueous phase equilibrium chemistry of vanadium oxide[57] and considering that the chemistry of vanadium coordination is pH

and V concentration dependent, the predominant species in the sole AMV aqueous solution will be $VO_2(OH)_2^-$ as well as $V_3O_9^{3-}$ at pH 3 to 7, and $V_{10}O_{28-x}(OH)_x^{(6-x)-}$ ions at higher V concentration. Moreover, the array of $V_{10}O_{28-x}(OH)_x^{(6-x)-}$ ion is lost when the AHM-AMV solution is diluted with water, i.e., up to a (AHM+AMV)/H_2O molar ratio of 1/70 (see Figure S1 in the Supporting Information). The equilibrium of vanadium species was altered and the new species in the resulting colourless AHM-AMV solution absorbs in the UV region. Hence, according to the diagram of equilibrium species for vanadium, tetrahedral oxo-alkoxo vanadate species $[VO_2(OH)_2]^-$ will be preferably formed in the diluted solution.[57] The transformation of vanadium polyoxometalate ions is accompanied by a change in the coordination of vanadium, from octahedral to a more isolated tetrahedral species. The two bands at 210 and 230 nm in Figure S1 correspond to the ligand to metal charge transfer (LMCT) transitions of terminal and bridging oxygen to vanadium, respectively.[53] It is clear then, the importance of maintaining an adequate AMV concentration to favour the presence of decavanadate ions in solution wherein V atoms are in octahedral coordination. These vanadium polyoxometalate ions, in turn, will generate the Mo and V Anderson-type polyoxometalate structure, which is the precursor of the MoVTeNb mixed oxide catalysts.[58,59]

More detailed information regarding the molybdenum and vanadium precursor solution was obtained from the corresponding Raman spectrum (Figure 2, spectrum b). The persistence of the absorption bands at 891 and 935 cm^{-1}, related to $[Mo_7O_{24}]^{6-}$ species, is also indicative of a weak interaction between Mo and V polyoxometalate ions at this step. Furthermore, the Raman spectrum of the pure, light yellow AMV solution at pH = 6.49 and 353 K shows a well-defined band at 942 cm^{-1} and a broad shoulder that extends from 850 to 930 cm^{-1} (Figure S2). Griffith and Lesniak[60] have assigned these bands to decavanadate ions $[V_{10}O_{28-x}(OH)_x]^{(6-x)-}$. At higher vanadium concentration, condensation occurs, which involves the nucleophilic addition of negatively charged $OH^{\delta-}$ groups on positive vanadium cations $V^{\delta+}$. The bands are related to the stretching vibration of V=O bonds and vibrations of V-O-V bonds of polymerized vanadium species linked to decavanadate ions $[V_{10}O_{28}]^{6-}$.[61] Therefore, the additional absorption bands located at 954 and 980 cm^{-1} in the AHM-AMV solution (Figure 2, spectrum b) can be associated to $[V_{10}O_{28}]^{6-}$ polyoxometalate. On the other hand, the shift of the absorption band of $[V_{10}O_{28}]^{6-}$, from 942 cm^{-1} in pure AMV solution (Figure S2) to 954 cm^{-1} in the MoV solution (Figure 2, spectrum b), can be associated to different hydration degrees of vanadium polyoxometalate, as a consequence of the relatively lower pH (5.28) in MoV solution compared to pure AMV solution (6.49). In fact, at a given concentration, $[V_{10}O_{28}]^{6-}$ is the main species in aqueous AMV solution at pH around 5.5, but depending on the final pH of solution, $[V_{10}O_{27}OH]^{5-} \leftrightarrow [V_{10}O_{26}(OH)_2]^{4-}$ could be mainly formed. Additionally, a small band is observed at 846 cm^{-1} in Figure 2b, which may correspond to stretching vibrations of Mo-O-V bonds thus indicating a certain degree of interaction between Mo and V in the mixed solution.

On the contrary, when hexa-oxo-telluric acid, $Te(OH)_6$ TA (0.078 $mmol_{TA}$/ ml_{H2O}) was added into AHM-AMV solution, the pH of the resulting solution was once again slightly increased to 5.5, changing also its colour, from light yellow to orange-red. As time progressed, the formation of a precipitate was also observed. The UV-Vis spectrum of this ternary solution presents two absorption bands centred at 354 and 475 nm (Figure 1c); it is clear that the incorporation of $Te(OH)_6$ changes the Mo, V and/or Mo-V ion species, promoting the formation of Mo-Te-O, V-Te-O and/or Mo-V-Te-O chemical species. As shown in Figure S3, the aqueous telluric acid solution (pH = 3.9), presents an absorption band at *ca.* 245 nm in the UV region. Thus, the absorption bands observed in the Mo-V-Te solution cannot be directly associated to the presence of telluric acid. Moreover, when the pH of telluric acid solution is adjusted to 2.3 with 0.1M nitric acid solution, a new band at 302 nm appears, whose intensity increases notably when pH is once again reduced to 1. According to the UV-Vis spectrum of HNO_3 aqueous solution (not shown), the absorption band at 302 nm corresponds to nitric acid species. Furthermore, the stretching and deformation modes of octahedral TeO_6 unit of telluric acid, i.e. $\mu1(A_{1g})$ symmetric stretch, $\mu2(E_g)$ and $\mu3(F_{1u})$ asymmetric stretch, $\mu4(F_{1u})$ asymmetric bending and $\mu5(F_{2g})$ symmetric bending][62] were not detected, suggesting that Te^{6+} species are totally incorporated into Mo and/or V species, forming the so-called polyoxometalates.[63] Taking into account the broadening of both UV-Vis absorption bands, i.e., the first one extending from 330 to 400 nm and the second one from 400 to 550 nm approximately, they could overlap the formation of some Anderson-type heteropolytellurate species. [59]

The Raman spectrum of the ternary Mo-V-Te solution (Figure 2c) displays absorption bands at 802, 896, 935 and 1000 cm^{-1}, which could be ascribed to diverse Te-V-O, Te-Mo-O and Mo-V-Te-O species that are concomitantly formed. For its resemblance with the powder Raman spectrum of the Anderson-type heteropolyanion $[TeMo_6O_{24}]^{6-}$ in the corresponding form of ammonium salt reported by I. L. Botto *et al.*, [64] bands at 937 and 899 cm^{-1} have been associated to an Anderson-type heteropolytellurate $[TeMo_6O_{24}]^{6-}$ with Mo atoms partially replaced by V atoms, as indicated by Trunschke *et al.* [50] In the present study, the absorption bands at 802 and 896 cm^{-1} may also correspond to these Anderson-type molybdenum-vanadium heteropolytellurates. Additionally, Yuhao *et al.* [65] have shown that the replacement of one Mo atom in $(NH_4)_6TeMo_6O_{24}\bullet 7H_2O$ by V atom shifted the stretching mode of the terminal M=O bonds from 946 to 990 cm^{-1}. Accordingly, the band at 1000 cm^{-1} could be ascribed to $(NH_4)_6TeMo_{6-x}V_xO_{24}\bullet 7H_2O$, probably with more than one Mo atom being replaced by V atoms. This band at 1000 cm^{-1} has also been assigned to $(H_xV_{10}O_{28})^{(6-x)-}$ species.[60] Likewise, in a very interesting NMR spectroscopic study of precursor solution of Mo-V-Te-Nb-O oxide catalyst, R. I. Maksimovskaya *et al.* [59] have identified the polyoxometalate $V_9TeO_{28}^{5-}$ anion, with a decavanadate structure, containing Te^{6+} in one of its two central positions; hence, the Raman band at c.a. 1000 cm^{-1} detected in the present study may also correspond to the presence of the polyoxometalate anion in the ternary Mo-V-Te solution. The

band at 935 cm^{-1}, which is located at the same position than the band of the AHM species, is probably associated to free heptamolybdate species in the ternary Mo-V-Te solution.

Finally, when niobium oxalate/oxalic acid solution (0.05 $mmol_{Nb}/mL_{H2O}$, pH=1.31) was added into Mo-V-Te solution, the pH of the resulting orange-coloured solution decreased to 3.2 and a yellow precipitate was formed immediately. The UV-Vis spectrum of the MoVTeNbO slurry (Figure 1, spectrum d) is very similar to that of the ternary Mo-V-Te solution detecting a slight decrease in the intensity of the absorption bands. When adjusting the pH to 2.5, the spectrum presented a more pronounced intensity decrease in the UV-Vis absorption bands without modifying its position (Figure 1, spectrum e). It is worth mentioning that the UV-Vis spectrum of the NbO_x-oxalic acid ($C_2H_2O_4$) mixture solution displayed an absorption band at 265 nm (Figure S4), which suggest, in agreement with the pH of this solution (pH of ca. 0.6), the presence of $NbO(C_2O_4)_2H_2O^-$ as predominant ionic species.[66-68] Apparently, the decrease in the absorbance bands of the ternary Mo-V-Te mixture solution is brought about by a dilution effect being accompanied by a bare modification of the hetero-poly-tellurate species. The precipitate formation would indicate a common ion effect of oxalate ligands and, at the same time, the occurrence of some chemical interaction of niobium oxalate with heteropolytellurate species. Raman analysis of the quaternary solution provides insightful information about this phenomenon. Thus, the absorption bands at 802, 896, 935 and 1000 cm^{-1}, characteristic of the Mo-V-Te solution (Figure 2, spectrum c), are not altered by NbO_x (Figure 2, spectra d and e) except for a decrease in intensity. This effect is more evident when adjusting the pH of the quaternary solution to 2.5 (Figure 2, spectrum e). In fact, some significant changes in the absorption Raman spectra are detected when comparing that related to the Nb-free sample (Figure 2, spectrum c) with those associated to the Nb-containing samples (Figure 2, spectra d and e). For instance, the absorption band at 896 cm^{-1} was slightly shifted into higher frequencies (903 cm^{-1}). Even more importantly, the development of two new absorption bands, at 943 and 948 cm^{-1}, are detected. These two new bands overlap with the one at 935 cm^{-1}, the later present in the Mo-V-Te solution (Figure 2, spectrum c); the resulting band broadening indicate that the Mo species are very likely associated to V, Te and/or Nb. When the pH of the quaternary solution was adjusted to 2.5 (Figure 2, spectrum e), the band at 943 cm^{-1} became the most important one. NMR spectroscopic study performed by Maksimovskaya *et al.* [60] showed that the addition of niobium oxalate into the Mo-V-Te solution leads to the formation of a gel of Nb_2O_5 with the concomitant production of VO_2^+ and MoO_2^{2+} oxalates. Considering these results, the absorption bands at 943 and 948 cm^{-1} may indicate the formation of VO_2^+ and MoO_2^{2+} oxalates.

On the other hand, in the extended Raman spectra of AHM-AMV-TA, AHM-AMV-TA-NbO_x (pH=3.6) and AHM-AMV-TA-NbO_x (pH=2.5) solutions (Figure 3), a band at 646 cm^{-1} appears when NbO_x is added into the ternary Mo-V-Te solution, *vide* Figure 3c. The intensity of this band, corresponding to the absorption band of telluric acid, increases as the pH of Mo-V-Te-Nb solution decreases from 3.6 to 2.5. As was described above, the change of colour as well as the precipitation process during the addition of niobium oxalate is an indication that chemical interaction between the oxalate ions and the Mo,V-containing polyoxotellurates formed in the Mo-V-Te solution occurs. However, the identification of telluric acid in the quaternary Mo-V-Te-Nb-O slurry shows that some fraction of Mo,V-containing polyoxotellurates reacts with oxalic ions to form VO_2^+ and MoO_2^{2+} oxalates, segregating some telluric acid. Based on the ratio of areas of the absorption band at 646 cm^{-1} of the $Te(OH)_6$ aqueous solution and that of ternary Mo-V-Te solution, it was estimated that about 50% of tellurium is segregated out of the latter solution when pH was adjusted to 2.5. As the absorption band of niobium oxalate at 567 cm^{-1} is no longer observed, $NbO(C_2O_4)_2H_2O^-$ ionic species have been fully transformed. Taking into account that the interpretation of the Raman spectrum of Mo-V-Te-Nb mixture is complex due to overlapping of bands from both solution and precipitate, niobium compounds, which are surely contained in the precipitate, were not clearly identified in the Raman spectrum of the slurry.

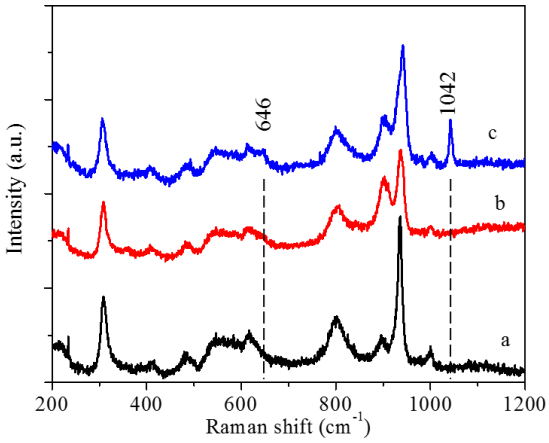

Figure 3. Extended Raman spectra of various solutions produced in the some preparation steps: a) AHM-AMV-TA, b) AHM-AMV-TA-NbO_x (pH=3.6) and c) AHM-AMV-TA-NbO_x (pH=2.5).

The influence of aging time on the structure of Anderson-type hetero-poly-tellurate was also analyzed. The optical profile of the UV-visible absorption edge of MoVTeNb slurry as a function of aging time is shown in Figure 4. A decrease in the absorption edge energy is observed, with the concomitant increase in the background of the spectrum upon increasing aging time. The optical absorption edge shifted from 2.30 eV to 2.10 eV in solutions aged for 15 and 240 minutes, respectively. Given that the absorption edge energy is sensitive to the nano-domain size and/or species concentration in solution, this behavior suggests the growth or agglomeration of the three dimensional polymeric polyoxometalate species of Mo-V-Te. Assuming that these Anderson type structures are preserved throughout drying and thermal activation processes, catalytically active multimetallic mixed oxide crystalline phases are certainly obtained.

Hence, the niobium addition to the Mo-V-Te solution appears to be a disruptive step in the catalyst preparation (due to the formation of a solid phase) because this visual behaviour is inherent to the Mo-V-Te-Nb-O catalysts prepared by the slurry method. It is worth noticing that the precipitated formed after the addition of Nb (i.e., Solid-1) presents a molar ratio equal to 1/0.20/0.25/0.56 for Mo/V/Te/Nb, whereas the Solid-2 produced by rotaevaporating the residual solution displays a chemical composition of 1/0.25/0.18/0.01 for Mo/V/Te/Nb. Such a difference in chemical composition indicates that most of Nb goes into the precipitated, which is agreement with the Nb role discussed above.

XRD and Raman of MoVTeNb catalysts

The two solids (Solid-1 and Solid-2) recovered in the synthetic procedure described in Section 2.1 were analysed to determine the distribution of chemical species and identify the corresponding crystalline structures via XRD analysis. Prior to the analysis, Solid-1 ad Solid-2 were thermally treated first at 523 K for 2 hours in static air, and then at 873 K for 2 hours under nitrogen flow. The thermally treated materials were, in a later stage, tested as catalyst in the ODH-E. The results related to these two materials were subsequently compared with those of the material produced by rotaevaporating the complete Mo-V-Te-Nb slurry (Solid-3), a procedure that is normally applied to prepare the Mo-V-Te-Nb-O mixed oxide catalyst. Notice that the chemical composition of Solid-3 was 1/0.24/0.24/0.18 for Mo/V/Te/Nb, values which are very close to the nominal atomic ratio employed in the synthesis, i.e. 1/0.24/0.24/0.19.

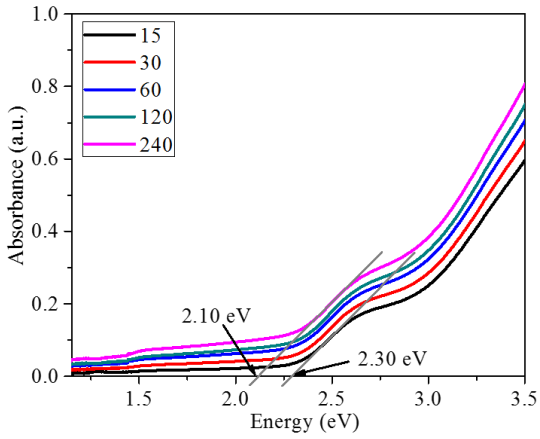

Figure 4. Optical profile of the UV-visible absorption edge of MoVTeNbO slurry as a function of aging time. Numbers associated to each line denote time in minutes.

The XRD patterns of the solids obtained from the precipitate (Solid-1) and that from the liquid fraction (Solid-2) are included in Figures 5 and 6, respectively. The appearance of diffraction peaks at 2θ = 6.5, 7.8, 9, 22.2 and 27.2° (Figure 5) clearly evidence, even if it is minority, the presence of the active M1 crystalline phase [ICDD, PFD 01-073-7574]. The M2 crystalline phase was also identified in this solid. Apart from these phases,

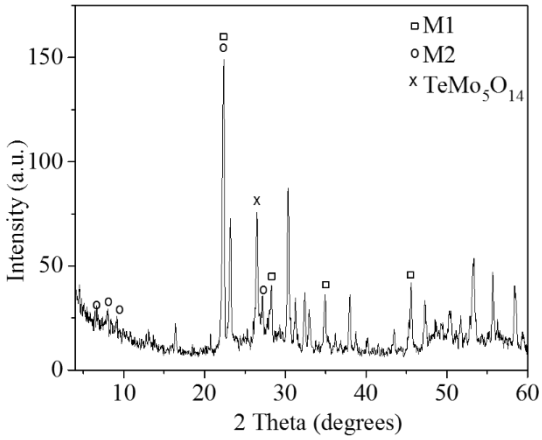

Figure 5. XRD pattern of Solid-1, material obtained from the precipitated fraction of Mo-V-Te-Nb slurry.

the peak at 2θ = 26.3° may indicate the formation of TeMo5O16 [ICDD PDF 02-031-0874]. Although the diffraction peaks located at 2θ = 16.2, 20.5 and 23.1° were not identified, they point to the presence of other extra crystalline phase.[50]

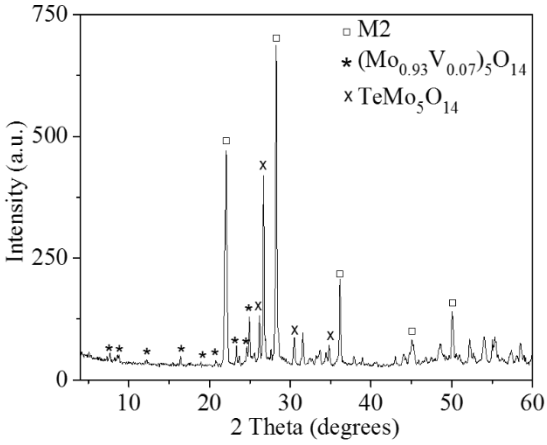

Figure 6. XRD pattern of Solid-2, material obtained by rotaevaporating the residual liquid fraction of Mo-V-Te-Nb slurry.

On the contrary, the material produced from the rotaevaporation of liquid phase of the Mo-V-Te-Nb slurry (Solid-2) exhibits diffraction peaks at 2θ = 22.1, 28.2, 36.4, 45.1 and 50.1° (Figure 6), which indicate the presence of the pseudo-hexagonal M2 crystalline phase [ICDD, PFD00-057-1099]. Meanwhile, the appearance of small peaks at 2θ =7.7, 8.7, 14.0, 23.3, 24.9, 29.7, 31.5, 32.4, and 33.5°, in addition to a peak at 2θ =22.1°, seems to be related to the formation of $(Mo_{0.93}V_{0.07})_5O_{14}$ [ICDD, PFD00-031-1437].[49,69] Furthermore, the coincidence of some diffraction peaks with some atomic plane distances of $TeMo_5O_{16}$ compound [ICDD, PFD 04-010-9132] also suggest the presence, to some extent, of this crystalline phase. Hence, from the XRD analysis of thermally treated materials

obtained from the liquid and solid fractions of Mo-V-Te-Nb slurry, it is evident that several crystalline phases are concomitantly produced during the synthetic procedure. It is worth noticing that the M1 crystalline phase is first generated in the precipitate of Mo-V-Te-Nb slurry, whose formation is enhanced by adding Nb. M2 crystalline phase, in contrast, is produced as the major phase from the liquid fraction of Mo-V-Te-Nb slurry.

Additionally, the XRD and Raman spectra of the catalyst obtained from the complete slurry of all the Mo, V, Te and Nb metal precursors (Solid-3) are shown in Figures 7 and 8, respectively. From the XRD point of view (Figure 7), after drying and treating thermally the whole Mo-V-Te-Nb slurry, a material

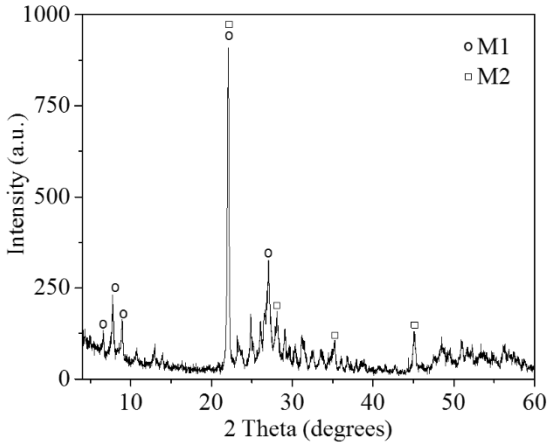

Figure 7. XRD pattern of Solid-3, the catalyst obtained from drying the complete Mo-V-Te-Nb slurry.

mainly containing M1 and M2 crystalline phases was produced. M1 is the major crystalline phase present in this material, with 95 wt% M1 *vs.* 5 wt% M2 crystalline phase, as determined by Rietveld refinement.[35] The Raman spectrum of Mo-V-Te-Nb sample (Figure 8) presents an intense band at 871 cm^{-1}, two wide shoulders at about 830 and 785 cm^{-1} and two other not well resolved bands at 457 and 475 cm^{-1}. The shape of this spectrum is very similar to that reported previously for these types of MoVTeNbO multimetallic mixed oxide materials, in other words, bands at 871, 830 and 475 cm^{-1} are related to M1 crystalline phase; whereas bands at 871, 785 and 457 cm^{-1} correspond to M2 crystalline phase.[33,35] The Raman spectrum of this material actually confirms the presence of both M1 and M2 crystalline phases in the final solid obtained from the whole slurry of mixed metals solution.

From the results discussed beforehand, it can be deduced that adding Nb favours the formation of M1 crystalline phase, which is observed in the precipitated obtained after Nb addition. Subsequently, when the whole slurry mixture is dried, an integration phenomena of aqueous species into the M1 structure takes place in view that in the Solid-2, which is obtained from the liquid phase, M2 is the dominant crystalline phase observed. This integration is incomplete because *ca.* 5 wt% of M2 crystalline phase is constituting the final solid (Solid-3).

Catalytic behaviour in the ODHE

Aimed to highlight the effect of the crystalline structures generated from the complete slurry produced out of the dissolution of Mo, V, Te and Nb salts on the catalytic properties

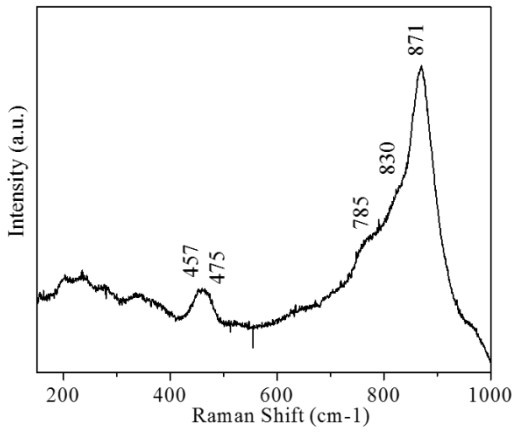

Figure 8. Raman spectra of Solid-3, the catalyst obtained from drying the complete Nb slurry.

of the final catalyst, the three solids produced from this metals slurry were evaluated in the oxidative dehydrogenation of ethane (ODHE). The reaction products spectra was in all cases limited to ethylene, CO and CO_2. Figure 9 displays a comparison of the catalytic performance, in terms of conversion of ethane and selectivity to ethylene, of the various catalysts subjected to reaction. The solid generated by thermal activation of Solid-1 exhibited a low ethane conversion, 4.2 %, a values that is threefold higher compared to the material obtained from liquid fraction (Solid-2), with a selectivity to ethylene as high as 96 %. Likewise, the liquid fraction of the slurry (i.e., Solid-2) and thermally activated at 873 K was practically inactive for ODHE at the reaction conditions outlined in Section 2.4, converting *ca.* 1.2 % of the fed ethane and selectivity to ethylene equal to 79 %.

The slightly higher ethane conversion of Solid-1 compared with that of Solid-2 appears to be associated to the presence of a small fraction of M1 crystalline phase in the later catalyst, whereas the higher selectivity to ethylene can be related to the presence of M1 as well as the absence of $(Mo_{0.93}V_{0.07})_5O_{14}$. Considering the relatively high amount of CO_x in the reactor effluent at the very low ethane conversion over Solid-2, the total combustion products would be related to the presence of $(Mo_{0.93}V_{0.07})_5O_{14}$ phase. It has been detected, in the case of catalytic materials presenting $(Mo_{0.93}V_{0.07})_5O_{14}$ phase, that the selectivity to CO_x always increases in detriment of that of ethylene (results not shown).[31] Finally, the material produced from the whole slurry (i.e., Solid-3) showed a substantially different catalytic behaviour, converting around 45 % of the fed ethane with a selectivity to ethylene as high as 89 %. Recall that this catalyst is mostly composed of M1 crystalline phase, with a minor amount of M2 phase. On the basis of these results, it is

concluded that the presence of the whole ensemble of metallic species in the slurry of Mo, V, Te and Nb is critical in the formation and chemical composition of the active and selective M1 crystalline phase as well other crystalline phases composing the final catalyst and the relative amount of them.

EXPERIMENTAL

Metal precursors solution

A slurry of Mo-V-Te-Nb mixed oxide catalyst precursors with a Mo/V/Te/Nb nominal atomic ratio of 1/0.24/0.24/0.19, was prepared according to the method described previously.[70] This multistage procedure can be resumed in the following steps: *i)* ammonium heptamolybdate (AHM, $(NH_4)_6Mo_7O_{24}\cdot 4H_2O$, Fluka) was dissolved in deionized water at 353 K; *ii)* wtammonium metavanadate (AMV, $NH_4VO_3\cdot xH_2O$, Sigma Aldrich) was then added with vigorous stirring into the AHM solution obtained in step *i*; *iii)* after 1 h of stirring, hexaoxotelluric acid (TA, $Te(OH)_6$, Aldrich) was incorporated into the AHM-AMV solution produced in stage *ii; iv)* afterwards, the AHM-AMV-TA solution was cooled down to 303 K producing solution A.

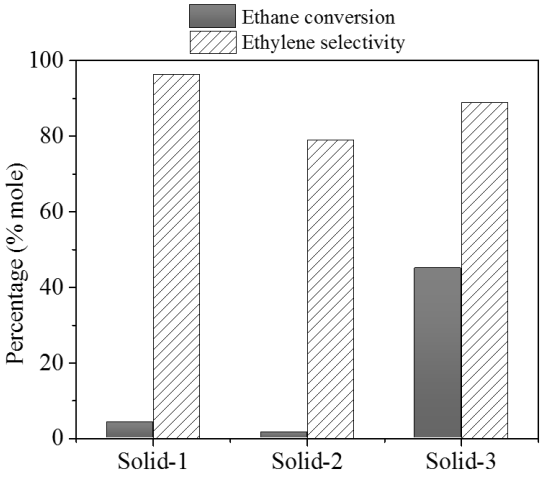

Figure 9. Catalytic properties in the ODHE of the three solid generated from the slurry of metals precursors. Experimental conditions: T= 673 K, space-time of 35 g_{cat} h $(mol_{ethane})^{-1}$.

In parallel, an aqueous solution of niobium ammonium oxalate ($C_4H_4NNbO_9\cdot xH_2O$, Aldrich, 20.32 wt% Nb) was prepared at 353 K, adding then oxalic acid (Aldrich, 99%) to produce a mixture referred to as solution B. After cooling down to room temperature, solution B was slowly added into solution A with continuous stirring, thus producing the AHM-AMV-TA-NbO_x solution with a pH of 3.6. 1M nitric acid was added into this solution to reduce the pH to 2.5 maintaining a vigorous stirring for 30 minutes. When mixing solution A and solution B, a precipitated was formed. This precipitate, which was separated by centrifugation, was designated Solid-1. Aside, the residual solution was rotaevaporated until recovering a powder that was labelled as Solid-2.

Preparation of the MoVTeNb catalyst

Aimed to obtain the MoVTeNbO multimetallic mixed oxide catalyst, the mixture of solution A and solution B containing the metal precursors, was rotaevaporated at 333 K and 42 kPa of vacuum. The obtained solid was next dried at 373 K for 12 h. Finally, the dried solid was thermally treated under nitrogen flow at 873 K for 2 h. The resulting material was coded as Solid-3.

Characterization of the metal solution and solids

Metals precursor solutions produced at each stage of the synthesis procedure described in Section 2.1, were examined using a Thermo® Scientific Evolution 600 UV/Vis Spectrophotometer, which was operated at room temperature within the wavelength range 190 to 700 nm.

The Raman spectra of the metal precursor solutions and the catalyst (Solid-3) were acquired using an YvonJobin (T64000) spectrometer equipped with a confocal microscope (Olympus, BX41) and an Ar ion laser operating at 514.5 nm at a power level of 10 mW. The spectrometer is equipped with a CCD camera detector.

The chemical composition of respective solids was determined by inductively coupled plasma atomic emission spectrometry (ICP-AES) in a Perkin–Elmer model Optima 3200 Dual Vision.

The X-ray powder diffraction patterns of solids were obtained in a Siemens D-500 diffractometer, provided with a θ-θ configuration and a graphite secondary beam monochrome. Diffraction patterns were measured from 4 to 60° using a 2θ step of 0.02° with 8 s per point, using Cu $K\alpha_{1,2}$ radiation with a wavelength of 1.5418 Å as well as a power of 40 kV and 40 Ma.

Catalytic performance evaluation

The catalytic properties of the various solids were evaluated in a lab-scale fixed-bed reactor made in quartz, which was operated isothermally, at atmospheric pressure and under integral regime. In all runs, the reactor was loaded with 0.6 g catalyst, selecting particles with an average size of 150 microns. The reaction mixture comprised ethane (C_2, 99.7 vol%), oxygen (O_2, 99.996 vol%) as well as nitrogen (N_2, 99.999 vol%). Experiments were carried out at 713 K, adjusting the $C_2/O_2/N_2$ nominal inlet molar ratio to 9/7/84 and varying the inlet flow rate to attain space-time values of 35 and 70 g_{cat} h $(mol_{ethane})^{-1}$. For mass balance purposes, the reactor effluent was analyzed periodically online by gas chromatography in a HP-7890 series II GC equipped with FID and TCD detectors and an array of three columns: a 30 m×530 µm×50 µm HP Plot Q capillary, a 30 m × 530 µm × 40 µm molecular sieve and a 30 m × 0.25 mm × 5 µm HP Plot alumina. Hydrocarbons were identified-quantified in FID, whilst the so-called permanent gases, i.e., CO_2, CO, O_2 and N_2, in the TCD. A blank experiment carried out at 713 K and the lowest inlet flow rate confirmed the absence of ethane conversion at these conditions. No catalyst deactivation was detected in any run. All catalytic responses included in this manuscript are given on carbon bases and correspond to steady-state values. Carbon balances in all cases were 100 ± 2.

Conclusions

MoVTeNbO multimetallic catalysts were successfully synthesized by slurry method from Anderson-type polyoxometalate precursor. The incorporation of hexaoxotelluric acid interacts with Mo, V and/or Mo-V ion species, inducing the formation of several chemical species such as Mo-Te, V-Te and/or Mo-V-Te, which promote the formation of an Anderson-type structure. The presence of vanadium polyoxometalate ions in octahedral environment is, however, necessary for its formation, which is influenced by V-concentration. Niobium oxalate induces the formation of a precipitate in which the M1 crystalline phase is initially formed. When liquid and precipitated fractions of the slurry were analysed separately, a small amount of M1 crystalline phase is observed in the precipitated fraction, which is not present in the liquid fraction. However, when the liquid and precipitated fractions are dried and thermally-treated together, the M1 phase is preferentially formed, constituting 95 wt% of the solid. Therefore, all Mo, V, Te and Nb chemical species participate as building blocks to obtain the active crystalline phase M1. When constituted mainly of M1 crystalline phase, the catalyst is very active in the ODHE reaction, converting 45 % of the fed ethane with a selectivity to ethylene of around 90 %. In contrast, when no M1 phase is present in the solid, the catalyst exhibits a very low capacity to convert the fed ethane, ca. 1.2%.

Conflicts of interest

There are no conflicts of interest to declare.

Acknowledgements

This work was financially supported by the Instituto Mexicano del Petróleo. EMF thanks CONACyT México and IMP (grant 63053) for scholarships. JMLN thanks also DGICYT in Spain (Porject CTQ2015-68951-C3-1-R).

Notes and references

1 T. Ushikubo, I. H. Nakamura, Y. Koyasu and S. Wajiki, *US Patent* 5 380 933, 1995.
2 T. Ushikubo, K. Oshima, T. Ihara and H. Amatsu, *US Patent* 5 534 650, 1996.
3 T. Ushikubo, K. Oshima, A. Kayo, M. Vaarkamp and M. Hatano, *J. Catal.,* 1997, **169**, 394.
4 T. Ushikubo, K. Oshima, A. Kayou and M. Hatano, *Stud. Surf. Sci. Catal.,* 1997,**112**, 473.
5 T. Ushikubo, *Catal. Today,* 2000, **57**, 331.
6 W. Ueda and K. Oshihara, *Appl. Catal. A: Gen.* 2000, **200**, 135.
7 H. Watanabe, Y. Koyasu, *Appl. Catal. A: Gen.,* 2000, **194-195**, 479.
8 H. Hinago, S. Komada and A.K. Kogyo, *US Patent* 6 063 728, 2000.
9 P. Botella, B. Solsona, A. Martinez-Arias, and J.M. López Nieto, *Catal. Lett.,* 2001, **74,** 149.
10 K. Oshihara, T. Hisan, and W. Ueda, *Top. Catal.* 2001, **15***,* 153.
11 P. Botella, J.M. López Nieto, B. Solsona, A. Mifsud, and F. Márquez, *J. Catal.,* 2002, **209**, 445.
12 J.M.M. Millet, H. Roussel, A. Pigamo, J.L. Duboi, and J.C. Jumas, *Appl. Catal. A: Gen*., 2002, **232,** 77.
13 P. DeSanto Jr, D.J. Buttrey, R.K. Grasselli, C.G. Lugmair, A.F. Volpe, B.H. Tob, and T. Vogt, *Top. Catal.,* 2003, **23,** 23.
14 J.M.M. Millet, M. Baca, A. Pigamo, D. Vitry, W. Ued, and J.L. Dubois, *Appl. Catal. A: Gen.,* 2003, **244,** 359.
15 P. Botella, E. García-González, A. Dejoz, J.M. López Nieto, M.I. Vázquez, and J. González-Calbet, *J. Catal.,* 2004, **225,** 428.
16 J. Holmberg, R.K. Grasselli, and A. Andersson, *Appl. Catal. A: Gen.,* 2004, **270,** 121.
17 R.K. Grasselli, D. J. Buttrey, P. DeSanto Jr., J.D. Burrington, C.G. Lugmair, A.F. Volpe Jr, and T. Weingand, *Catal. Today,* 2004, **91-92,** 251.
18 a) W. Ueda, D. Vitry, T. Katou, *Catal. Today,* 2005, **99,** 43; b) H. Murayama, D. Vitry, W. Ueda, G. Fuchs, M. Ann, and J.L. Dubois, *App. Catal. A: Gen,* 2007, **318,** 137.
19 V.V. Guliants, R. Bhandari, B. Swaminathan, V.K. Vasudevan, H.H. Brongersma, A. Knoester, A.M. Gaffney, and S. Han, *J. Phys. Chem. B*, 2005, **109,** 24046.
20 R.K. Grasselli, D.J. Buttrey, J.D. Burrington, A. Andersson, J. Holmberg, W. Ueda, J. Kubo, C.G. Lugmai, and A.F. Volpe Jr., , *Top. Catal.,* 2006, **38,** 7.
21 O.V. Safonova, B. Denia, and J.M.M. Millet, *J. Phys. Chem. B,* 2006, **110-47,** 23962.
22 J.B. Wagner, O. Timpe, F.A. Hamid, A. Trunschke, U. Wild, D.S. Su, R.K. Widi, S.B.A. Hami, and R. Schlögl, *Top. Catal.* 2006, **38,** 51.
23 Y.V. Kolen'ko, W. Zhang, R.N. d'Alnoncourt, F. Girgsdies, T.W. Hansen, T. Wolfram, R. Schlögl and A. Trunschke, *ChemCatChem.,* 2011, **3,** 1597.
24 M. Hävecker, S. Wrabetz, J. Kröhnert, L.I. Csepei, R.N. d'Alnoncourt, Y.V. Kolen'ko, F. Girgsdies, R. Schlög, and A. Trunschke, *J. Catal.,* 2012, **285,**48.
25 S. Ishikawa, M. Tashiro, T. Murayama, and W. Ueda, *Cryst. Growth Des.,* 2014, **14-9,** 4553.
26 a) J.M. López Nieto, P. Botella, M.I. Vázquez, and A. Dejoz, *Patent* WO 2003064035 A1, 2003; b) J.M. López Nieto, P. Botella, M.I. Vázquez, and A. Dejoz, *U.S. Patent* 7319179 B2, 2008.
27 J.M. López Nieto, P. Botella, M.I. Vázquez, and A. Dejoz, *Chem. Commun.*, 2002, 1906.
28 J.M. López Nieto, P. Botella, P. Concepción, A. Dejoz and M.I. Vázquez, *Catal. Today,* 2004, ***91-92,*** 241.
29 F. Ivars, P. Botella, A. Dejoz, J.M. López Nieto, P. Concepción and M.I. Vázquez, *Top. Catal.,* 2006, **38,** 59.
30 Q. Xie, L. Chen, W. Weng and H. Wan, *J. Mol. Catal. A,* 2005, **240,** 191.
31 P. Botella, A. Dejoz, M.C. Abello, M.I. Vazquez, L. Arrua and J.M. Lopez Nieto, *Catal. Today,* 2009, **142,** 272.
32 B. Deniau, J.M.M. Millet, S. Loridanta, N. Christin and J.L. Dubois, *J. Catal.,* 2008, **260,** 30.
33 B. Solsona, M.I. Vázquez, F. Ivars, A. Dejoz, P. Concepción and J.M. López Nieto, *J. Catal.,* 2007, **252,** 271.
34 a) T.T. Nguyen, L. Burel, D. L. Nguyen, C. Pham-Huu and J.M.M. Millet, *Appl. Catal. A: Gen,* 2012, **433-434,** 41; b) T.T. Nguyen, M. Aouine and J.M.M. Millet, *Cat. Commun.,* 2012, **21,** 22.
35 J.S. Valente, H. Armendáriz-Herrera, R. Quintana-Solórzano, P. del Ángel, N. Nava, A. Massó and J.M. López Nieto, *ACS Catal.,* 2014, **4,** 1292.
36 E.M. Thorsteinson, T.P. Wilson, F.G. Young and P.H. Kasai, *J. Catal.* 1978, **52,** 116.
37 a) S. Ishikawa, X. Yi, T. Murayama and W. Ueda, *Appl. Catal. A: Gen,* 2014, **474,** 10; b) S. Ishikawa, X. Yi, T. Murayama and W. Ueda, *Catal. Today,* 2014, **238,** 35.

38 R.K. Grasselli, J.D. Burrington, D.J. Buttrey, P. DeSanto Jr., C.G. Lugmair, A.F. Volpe Jr. and T. Weingand, *Top. Catal.,* 2003, **23,** 5.
39 R.K. Grasselli, C.G. Lugmair, A.F. Volpe Jr., A. Andersson and J.D. Burrington, *Catal. Today,* 2010, **157**, 33.
40 R.K. Grasselli, C.G. Lugmair and A.F. Volpe Jr., *Top. Catal.,* 2011, **54,** 595.
41 R.K. Grasselli, *Catal. Today* 2014, ***238,*** 10.
42 I. Ramli, P. Botella, F. Ivars, W.P. Meng, S.M.M. Zawawi, H.A. Ahangar, S. Hernández and J.M. López Nieto, *J. Mol. Catal. A,* 2011, **342,** 50.
43 F.N. Naraschewski, C. Praveen Kumar, A. Jentys and J.A. Lercher, *Appl. Catal A*, 2011, **391,** 63.
44 T. Blasco, P. Botella, P. Concepción, J. M. López Nieto, A. Martinez-Arias and C. Prieto, *J. Catal.,* 2004, **228,** 362.
45 X.J. Yang, R.M. Feng, W.J. Ji and C.T. Au, *J. Catal.* 2008, **253,** 57.
46 A.M. Gaffney, S. Chaturvedi, M.B. Clark Jr., S. Han, D. Le, S.A. Rykov and J.G. Chen, *-J. Catal.,* 2005, **229,** 12.
47 L. Espinal, K.A. Malinger, A. E. Espinal, A.M. Gaffney and S.L. Suib, *Adv. Funct. Mater.,* 2007, **17,** 2572.
48 Y.V. Kolen´ko, K. Amakawa, R.N. d'Alnoncourt, F. Girgsdies, G. Weinberg, R. Schlögl and A. Trunschke, *ChemCatChem.,* 2012, 4, 495.
49 a) P. Concepcion, S. Hernandez and J.M. Lopez Nieto, *App. Catal. A*, 2011, **391,** 92; b) P. Botella, E. Garcia-Gonzalez, J.M. Lopez Nieto, J.M. Gonzalez-Calbet, Solid State Sci. 2005, **7,** 507.
50 P. Beato, A. Blume, F. Girgsdies, R. E. Jentoft, R. Schlogl, O. Timpe, A. Trunschke, G. Weinberg, Q. Basher, F. A. Hamid, S.B.A. Hamid, E. Omar and L. Mohd Sali*, Appl. Catal. A: Gen,* 2006, **307,** 137.
51 A. Celaya Sanfiz, T.W. Hansen, F. Girgsdies, O. Timpe, E. Rödel, T. Ressler, A. Trunschke and R. Schlögl, *Top. Catal.,* 2008, **50,** 19.
52 T. Ozeki, H. Kihar, and S. Ikeda, *Anal. Chem.,* 1988, **60,** 2055.
53 K.H. Tytk, and B. Schönfeld, *Z. Naturforsch*, 1975, **30b,** 471.
54 S. Çaki, and E. Biçer, *J. Chil. Chem. Soc.,* 2010, **55,** 236.
55 A. Müller, E. Krickemeyer, H. Bögge, M. Schmidtman, and F. Peters, *Angew. Chem. Int. Ed.,* 1998, **37,** 3359.
56 J. Livage, *Materials* 2010, **3,** 4175.
57 C.F. Baes Jr and R.E. Mesmer in *The Hydrolysis of Cations*; Wiley N.Y., 1970.
58 H. Tsuji and Y. Koyasu, *J. Am. Chem. Soc.* 2002, **124,** 5608.
59 R.I. Maksimovskaya, V.M. Bondareva and G.I. Aleshina, *Eur. J. Inorg. Chem.,* 2008, 4906.
60 W.P. Griffith and P.J.B. Lesniak, *J. Chem. Soc. A,* 1969, 1066.
61 Z. Luan, P.A. Meloni, R.S. Czernuszewicz and L. Kevan, *J. Phys. Chem. B,* 1997, **101,** 9046.
62 I.S. Butler, H.A. M. El-Sherbeny, I.M. Kenawy and S.I. Mostafa, *J. Mol. Struc.,* 2013, **1036,** 510.
63 A. Müller, P. Kögerler and A.W.M. Dress, *Coord. Chem. Rev.,* 2001, **222,** 193.
64 I.L. Botto, C.I. Cabello and H.J. Thomas, Studies. *Mater. Chem. Phys.,* 1997, **47,** 37.
65 Y. Sun, J. Liu and E. Wang, *Inorg. Chim. Acta,* 1986, **117,** 23.
66 H. Yoshida, T. Tanaka, T Yoshida, T. Funabiki and S. Yoshida, *Catal. Today,* 1996, **28,** 79.
67 Y. Kubouchi, S. Hayakawa, H. Namatame and T. Hirokawa, *X-Ray Spectrometry*, 2012, **41**, 259.
68 D. Prasetyoko, Z. Ramli, S. Endud and H. Nur, *Mater. Chem. Phys.,* 2005, **93,** 443.
69 T. Konya, T. Katou, T. Murayama, S. Ishikawa, M. Sadakane, D. Buttrey and W. Ueda, *Catal. Sci. Technol.,* 2013, ***3,*** 380.
70 J.M. Oliver, J.M. López Nieto, P. Botella and A. Mifsud, *Appl. Catal. A: Gen.,* 2004, **257,**67.